UC Irvine
UC Irvine Previously Published Works

Title

Oxygen Reduction Reaction Electrocatalysts Derived from Iron Salt and Benzimidazole and Aminobenzimidazole Precursors and Their Application in Microbial Fuel Cell Cathodes.

Permalink

https://escholarship.org/uc/item/7zd312hz

Journal

ACS Applied Energy Materials, 1(10)

Authors

Mecheri, Barbara
Gokhale, Rohan
Santoro, Carlo
et al.

Publication Date

2018-10-22

DOI

10.1021/acsaem.8b01360

Peer reviewed

Oxygen Reduction Reaction Electrocatalysts Derived from Iron Salt and Benzimidazole and Aminobenzimidazole Precursors and Their Application in Microbial Fuel Cell Cathodes

Barbara Mecheri,*,† Rohan Gokhale,‡ Carlo Santoro,*,‡ Maida Aysla Costa de Oliveira,† Alessandra D'Epifanio,† Silvia Licoccia,† Alexey Serov,‡ Kateryna Artyushkova,‡ and Plamen Atanassov‡

†Department of Chemical Science and Technologies, University of Rome Tor Vergata, Via della Ricerca Scientifica, 00133, Rome, Italy

‡Department of Chemical and Biological Engineering, Center for Micro-Engineered Materials (CMEM), Advanced Materials Lab, University of New Mexico, 1001 University Blvd. SE Suite 103, MSC 04 2790, Albuquerque, New Mexico 87131, United States

ABSTRACT: In this work, benzimidazole (BZIM) and aminobenzimidazole (ABZIM) were used as organic-rich in nitrogen precursors during the synthesis of iron−nitrogen−carbon (Fe−N−C) based catalysts by sacrificial support method (SSM) technique. The catalysts obtained, denoted Fe-ABZIM and Fe-BZIM, were characterized morphologically and chemically through SEM, TEM, and XPS. Moreover, these catalysts were initially tested in rotating ring disk electrode (RRDE) configuration, resulting in similar high electrocatalytic activity toward oxygen reduction reaction (ORR) having low hydrogen peroxide generated (<3%). The ORR performance was significantly higher compared to activated carbon (AC) that was the control. The catalysts were then integrated into air-breathing (AB) and gas diffusion layer (GDL) cathode electrode and tested in operating microbial fuel cells (MFCs). The presence of Fe−N−C catalysts boosted the power output compared to AC cathode MFC. The AB-type cathode outperformed the GDL type cathode probably because of reduced catalyst layer flooding. The highest performance obtained in this work was $162 \pm 3 \ \mu Wcm^{-2}$. Fe-ABZIM and Fe-BZIM had similar performance when incorporated to the same type of cathode configuration. Long-term operations show a decrease up to 50% of the performance in two months operations. Despite the power output decrease, the Fe-BZIM/Fe-ABZIM catalysts gave a significant advantage in fuel cell performance compared to the bare AC.

KEYWORDS: oxygen reduction reaction, PGM-free catalyst, catalyst kinetics, sacrificial support method, microbial fuel cell
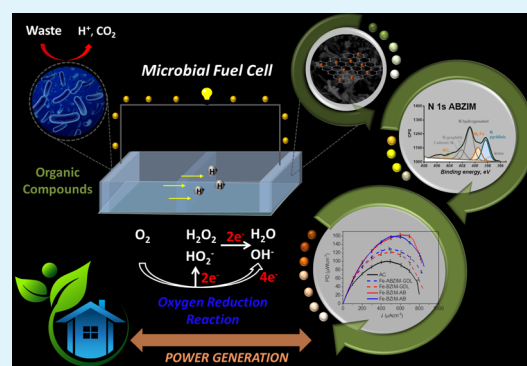
1. INTRODUCTION

Microbial fuel cell (MFC) is an interesting technology that combines several aspects, such as microbiology, electrochemistry, chemistry, physics, and engineering, within a device that is capable of degrading organic pollutants and producing useful electricity at ambient conditions (atmospheric pressure and $T \sim 15-30$ °C).[1,2] The used organics are an essential component of energy generation and are the bacterial feeding (fuel) for the oxidation reaction.[3,4]

In general, the organics are electro-oxidized into carbon dioxide, protons, and electrons by the bacterial catalyst, which is composed of electroactive microorganisms.[5−7] Those specific bacteria colonize the anode electrode and can release the electrons from the oxidation reaction directly to the electrically conductive electrode, while protons are simultaneously released into the solution.[5−7] Electrons move through the external circuit generating electron flow and by that useful electricity. The electrochemical reduction reaction occurs at the cathode in which an oxidant is reduced.[1,2] Among several

available oxidants, oxygen is the most used one, and this choice is justified by several reasons, and among them, the more important are the high electrochemical potential and natural availability in the air at no additional cost.[8]

Despite several practical implementations with MFCs have been recently presented,[9−12] bioelectrochemical systems suffer from very low power density output that has to be improved for practical applications. The cathode reduction reaction is the limiting step for almost all the bioelectrochemical systems.[13,14] The oxygen reduction reaction (ORR) in neutral media is severely limited by the electrolyte pH, high activation overpotentials and sluggish kinetics.[15,16] Therefore, the addition of the catalyst is critically important to accelerate the slow kinetics of ORR process.[1,2] Bacterial catalysts, despite being inexpensive, suffer from low turnover frequency (TOF),

and the mechanism of the oxygen electroreduction is still debated.[17−19] On the other side, enzymes, such as laccase[20−23] or bilirubin oxidase,[20−23] are excellent ORR catalysts in neutral media, but their low durability and the elevated cost discourages the utilization for real industrial applications.[24,25]

Abiotic catalysts are the most preferred catalysts to be adopted in MFC devices because, with the exclusion of platinum group metals (PGMs), these catalysts are durable in long terms operation, resistant to the majority of pollutants and with the affordable price the overall capital cost of the system becomes commercially viable.[26−29] It is well-known that platinum is a rare and expensive metal, which can be easily poisoned in a polluted environment and consequently is not suitable for MFCs applications.[30−32] As a matter of fact, Pt was the most used catalyst in MFCs for several years however this choice was mainly dictated by the fact that Pt catalysts were heavily studied and used in acidic and alkaline fuel cells, technologies that are more mature compared to MFCs systems.[29,33,34] Pt has been recently substituted by materials that are potentially cost-effective and moreover are durable in harsh and contaminated environments.[27−29]

Few recent reviews have focused on the topic of alternative catalyst to Pt.[27−29] Various carbonaceous materials have been investigated successfully as cathode catalysts in MFCs.[1,2,35−37] The investigations varied from activated carbon that is commercially available at relatively low cost to modified activated carbon or carbon black modified with nitrogen functional groups.[38−46] Other, even more, sophisticated and lab-made carbonaceous materials such as aerogel,[47] carbon nanotubes (CNT),[48] carbon nanofibers (CNF),[49] and graphene[50−53] have also been recently evaluated, providing relatively high power output despite their cost is relatively higher compared to commercial AC. Unfortunately, as mentioned above carbon-based materials still carry on the majority of drawbacks for ORR such as high overpotential and low kinetics that are typical for cathodic catalysts operating in neutral media.[1,2,13,54] In the past 10 years or so, catalysts based on earth-abundant transitional metals have been exploited with more and more devotion and attention.[27−29] Those catalysts are named platinum group metal-free catalysts and abbreviated as PGM-free. Some classes of PGM-free catalysts are based on macrocyclic organic molecules with incorporated earth abundant transitional metals (e.g., porphyrins,[55,56] phthalocyanines,[57−59] etc.) or materials based on pyrolyzed organic compounds mixed with transitional metals.[60−65] The latter materials are preferred because of the cheaper manufacturing procedure. The earth-abundant metals utilized during pyrolysis process and investigated as a catalyst for ORR in neutral media are manganese (Mn),[58,66−68] iron (Fe),[69−77] cobalt (Co),[55,78−80] and nickel (Ni),[81,82] Other metals, such as copper (Cu),[83] zirconium (Zr),[84] etc., have also been investigated for ORR in MFCs. It was shown unanimously that the best performing PGM-free catalyst was based on iron[85,86] that was showed also to be superior compared to platinum.[32] In several investigations, iron showed higher performance compared to cobalt.[85−87] Mn, Ni, Zr, and Cu showed inferior performance despite having much higher electroactivity compared to bare AC.[82,83,85] In general, PGM-free ORR catalysts have attracted the attention of the MFC's world due to the utilization of abundant metals that do not have excessive cost with the advantage of at least doubling the performance of bioelectrochemical systems that struggle in electrochemical output to be utilized for real applications.

In this work, iron-based catalysts were synthesized using iron salt, as well as benzimidazole and aminobenzimidazole as nitrogen-rich organic precursors (N−C source) and comprehensively investigated. Sacrificial support method (SSM) was used during the synthesis incorporating silica as a template during the high-temperature pyrolysis process and removing it afterward. The catalysts obtained were based on atomically dispersed transition metals coordinated with nitrogen inside of 3D carbon matrix. The kinetics performance in oxygen reduction reaction of the catalysts was studied first in rotating ring disk electrode (RRDE) in neutral media. Electrochemical parameters of interest, such as onset potential, half wave potential, limiting current, hydrogen peroxide generation, and electron transfer mechanism, were investigated. Furthermore, these catalysts were integrated into an air-breathing cathode and tested at microbial fuel cell conditions. The obtained polarization curves and power curves were analyzed and discussed in the present article.

2. MATERIALS AND METHOD

2.1. Catalyst Preparation. Two PGM-free Fe−N−C catalysts were prepared using a sacrificial support method (SSM). The same method was proposed to synthesize several catalysts previously presented.[88−90] Iron nitrate (as a metal source) was mixed either with benzimidazole (BZIM) or aminobenzimidazole (ABZIM), respectively (as N−C source), and then also with monodispersed silica used as a sacrificial template. The mixture was pyrolyzed at controlled temperature furnace at 900 °C. The powder was inserted into a quartz tube flushed with UHP nitrogen (flow of 100 cm^3 min^{-1}). After 45 min at a stable temperature (900 °C), the quartz tube was removed from the hot zone of the furnace and cooled down until room temperature was reached. After this procedure, the powder was treated with HF (∼24 wt % in H_2O) to remove the silica template, unreacted iron or iron compounds (oxides, carbides, and carbonitrides) as well as to create a three-dimensional structure. Further, the powder was thoroughly washed with water to remove HF, H_2SiF_4, FeF_x and then dried at 80 °C overnight. The final step of catalysts preparation consisted in ball milling of Fe−N−C powders in planetary ball-mill at 450 rpm for t = 20 min.

2.2. Morphological Analysis and Surface Chemistry Analysis. The morphological features of the synthesized catalysts were investigated using scanning electron microscopy (SEM) and transmission electron microscopy (TEM). SEM images were taken using Hitachi S-5200 Nano SEM with an accelerating voltage of 10 keV. Transmission electron microscopy (TEM) images were obtained using JEOL JEM-2010. The surface chemistry of the catalysts was obtained using X-ray photoelectron spectroscopy (XPS). The XPS instrument utilized for these measurements was a Kratos Axis Ultra DLD XPS with a monochromatic Al Kα source operating at 225 W. Three independent areas for each specific catalyst were analyzed, and the average is presented. Specifically, high-resolution C 1s and N 1s were acquired with a pass energy of 20 eV. Being the surfaces analyzed conductive, no additional charge compensation was adopted. CASAXPS software was used for processing XPS spectra. 70% Gaussian/30% Lorentzian [GL(30)] line shape was utilized to fit the curves.

2.3. Rotating Ring Disk Electrode (RRDE) Experiments. Rotating ring disk electrode (RRDE) method was used to study the catalyst kinetics toward ORR in neutral media. Two loadings of each catalyst were prepared on the working electrode (WE) (0.1 and 0.6 mg cm^{-2}), while activated carbon (AC) was used as a control. The RRDE inks were prepared by mixing of 5 mg of each catalyst with 0.85 mL of IPA: H_2O solution (ratio (4:1)) and 0.15 mL 0f 0.5 wt % of Nafion solution. The mixture was ultrasonicated for 1 min for at least three times to obtain a uniform dispersion of the solid catalyst in IPA:H_2O:Nafion solution. These inks were deposited on the WE surface (glassy carbon, the area of 0.2472 cm^2) using a precision micropipette and allowed to dry at room temperature on air. The

platinum ring of RRDE tip had a surface area of 0.1859 cm^2. The electrolyte used in the present work consisted of potassium phosphate buffer (with a pH of 7.5) with the addition of 0.1 M KCl. The electrolyte was purged for at least 20 min with pure oxygen before the electrochemical ORR measurements, to obtain complete oxygen saturation of the media. All RRDE experiments were done at disk speed rotation of 1600 rpm. Two Pine potentiostats were used to measure the disk and ring currents during the experimentation. Linear sweep voltammetry (LSV) was run in a potential window between 0.4 and −0.7 V (vs Ag/AgCl) at a scan rate of 5 mV s^{-1} using three-electrodes configuration with the disk connected to the working channel (WE), a graphite rod as the counter electrode and a Ag/AgCl 3 M KCl reference electrode connected to the reference channel.

2.4. Preparation of Fe−N−C MFC Cathodes. Along with the RRDE tests, the realistic electrochemical experiments evaluating the catalytic activity of the PGM-free catalyst were conducted in fuel cell conditions. To perform such types of measurements, Fe-ABZIM and Fe-BZIM were integrated into two different types of cathodic catalyst layers: air-breathing electrode and gas diffusion layer cathode, followed by MFC tests.

2.4.1. Air-Breathing Cathodes. The air-breathing cathodes were prepared as follows. Activated carbon (AC), polytetrafluorethylene (PTFE), and carbon black (CB, Alfa Aesar, acetylene 50% compressed) with the ratio of 7:2:1 were blended for 5 min, using a method previously established.[91,92] The obtained black powder was placed on top of a stainless-steel (SS) mesh, followed by insertion of mesh + powder inside of a metallic pellet press die. The die was assembled with punch and electrode was formed from powder at a pressure of 2 mT for a time of 5 min using a hydraulic press (Carver, USA). All the operations were conducted under normal conditions. The obtained cathode was denoted AC and did not contain an additional Fe−N−C catalyst. The AC/CB/PTFE in the electrode was 40 mg cm^{-2}. In parallel, in the case of Fe-contained catalysts, on the above mixture was added Fe-BZIM and Fe-ABZIM respectively. The electrode mixtures were homogenized manually by mixing AC/CB/PTFE and the Fe−N−C catalyst using a spatula. After mixing air-breathing electrodes were constructed by pressing following the procedure described above. In later cases, the loading of Fe−N−C ORR catalyst was 2 mg cm^{-2}, while keeping loading of AC/CB/PTFE at the same level (40 mg cm^{-2} of which 8 mg cm^{-2} PTFE). These air-breathing cathodes were labeled as Fe-BZIM-AB, Fe-ABZIM-AB, and AC.

2.4.2. Gas Diffusion Layer Cathodes. The gas diffusion layer (GDL) cathodes were prepared as follows. Carbon cloth GDLs (ELAT LT1400W MPL (Microporous Layer) treated, *FuelCellsEtc*, US) were modified by brush painting with a PTFE diffusion layer on the opposite side of MPL, as previously described.[74−76,84] After that, the catalyst layer was applied on the opposite side of the PTFE layer side by brush painting a 0.185 mg mL^{-1} suspension of either Fe-BZIM or Fe-ABZIM in a solution of 2-propanol (31 vol %), DI, 7.5 vol %), and Nafion perfluorinated solution (274704, Aldrich, 61.5 vol %): The loading of Fe-based catalyst was 2 mg cm^{-2} to match the catalyst amount deposited in the case of air-breathing cathodes, while PTFE loading was 13.4 mg cm^{-2}. The obtained gas diffusion layer cathodes are labeled as Fe-BZIM-GDL and Fe-ABZIM-GDL.

2.5. Microbial Fuel Cell Operations. The MFC reactor was made of a single cylindrical chamber with 28 mL as empty liquid volume, and 4 cm was the length of the cylinder.[74−76] The anode consisted of a graphite fibers brush with two twisted titanium wires as a core (2.5 cm length, 0.22 m^2 total surface area), and the cathode was a disk of either carbon cloth or stainless steel modified with the catalyst layer having a diameter of 3.8 cm. The cathode active surface area exposed to the liquid electrolyte was 7 cm^2. In the case of GDL cathodes, the PTFE layer faced the air-side, and the catalyst layer was in contact with the solution. In parallel, in the case of the air-breathing cathodes, the SS mesh faced the air-side while the catalyst layer faced the liquid.

MFCs were first acclimated and fed with 50 mM phosphate buffer aqueous solution (2.29 g L^{-1} Na$_2$HPO$_4$, 1.23 g L^{-1} NaH$_2$PO$_4$, 0.16 g L^{-1} NH$_4$Cl, and 0.07 g L^{-1} KCl; pH = 7) containing 1 g L^{-1} of

sodium acetate. Cathode and anode were connected with titanium wire, and the voltage was measured through an external resistance of 1 kΩ every 15 min using a multimeter (2700; Keithley, USA). Feeding solutions were replaced when the voltage dropped below 40 mV, forming one complete cycle of operation. All MFC tests were carried out at room temperature (T = 22 ± 3 °C) in two independent replicates for each cathode.

2.6. Electrochemical Analysis of MFCs Experiments. Electrochemical experiments were performed using a multichannel VSP potentiostat/galvanostat (BioLogic, France), and data were acquired by using the EC-Lab software. The tests were carried out using either a two-electrode configuration with the cathode connected to the working electrode channel and the anode connected to the counter electrode channel short-circuited with the reference electrode channel. Anode and cathode potentials were recorded separately and referred to the reference electrode (saturated calomel electrode, SCE). The polarization curves were recorded through linear sweep voltammetry (LSV) at a scan rate of 1 mV s^{-1}. The power density and current density generated by MFCs were normalized according to the cathode geometric surface area. Electrochemical impedance spectroscopy measurements were carried out in the frequency range of 0.1 Hz−100 kHz with 10 mV amplitude of the alternating current signal.

3. RESULTS AND DISCUSSION

3.1. Morphology and Surface Chemistry. SEM images evidence a porous morphology for both Fe-ABZIM and Fe-BZIM, as a result of the etching of the silica template during catalyst preparation (Figure 1a−c). The presence of iron
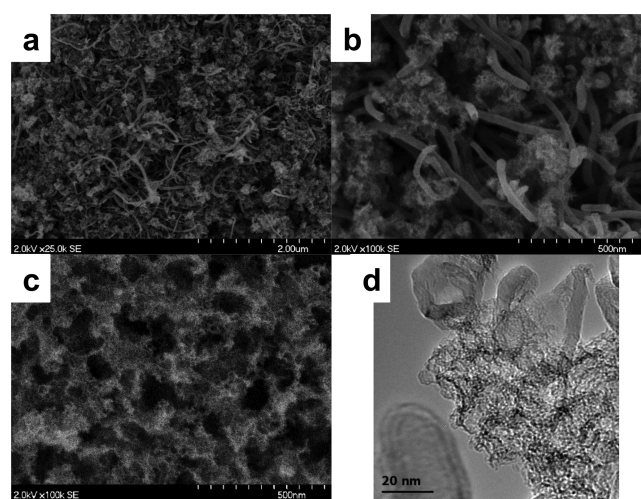

Figure 1. SEM images of Fe-BZIM (a, b) and Fe-ABZIM (c) catalysts and TEM image of Fe-BZIM (d) material.

nanoparticles in the final catalysts was not observed by TEM analysis (Figure 1d). Even more, it can be clearly seen on Figure 1d that etching procedure described above was effective in dissolving bulk iron species, leaving only concentric rings of highly graphitized carbon (Figure 1d). Overall, the morphology of Fe-BZIM and Fe-ABZIM was similar to other M−N−C materials prepared by sacrificial support method.[93,94]

The XPS analysis showed a very similar elemental composition of the two catalysts, which consist of carbon, oxygen, nitrogen, and iron (Figure 2). The catalysts had over 90% composition of elemental carbon, between 6.0% and 6.7% of oxygen and 2.8% of nitrogen. As expected, Fe was only in the small percentage of 0.2% for Fe-ABZIM and 0.1% for Fe-BZIM (Table 1). The small percentage was due to the etching with HF during the SSM synthesis process, as it was also
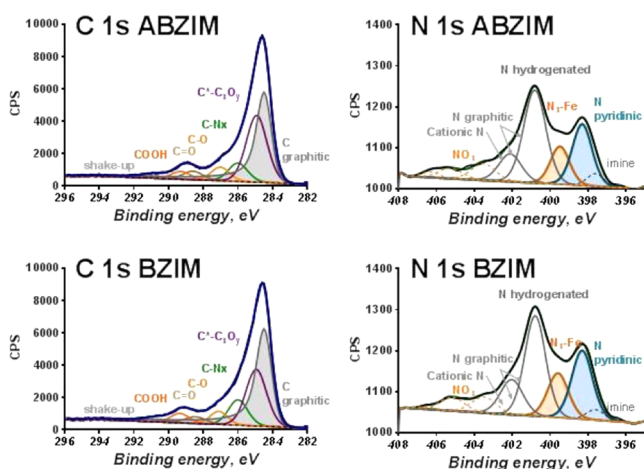
Figure 2. C 1s and N 1s XPS spectra of Fe-ABZIM and Fe-BZIM materials.

confirmed by analysis of TEM micrographs. As far as nitrogen speciation is concerned, the relative percentage of pyridinic and hydrogenated nitrogen atoms is the highest of all types of nitrogen atoms (Figure 2 and Table 1). Both samples also have very similar amounts of graphitic carbon and carbon surface oxides. It was shown before that pyridinic nitrogen and nitrogen coordinated to metal are species of extreme importance for ORR in acidic, neutral, and alkaline media.[69,95]

3.2. RRDE Experiments Results. Rotating ring disk electrode (RRDE) technique was used to study the catalyst oxygen electroreduction kinetics and measure the H_2O_2 yield produced during the tests. H_2O_2 is an intermediate product of incomplete oxygen reduction and therefore is undesired during the ORR process. Finally, knowing the disk and the ring current, it was possible to determine the electron transfer number related to the mechanism of ORR. Two catalyst loadings on WE were studied to determine the effect of a catalyst layer thickness on ORR kinetics.

Disk current recorded underlined a well-defined trend of the electrocatalytic activity showing that Fe−N−C catalysts were significantly more active toward ORR compared to AC (Figure 3a). This trend was independent of the used catalyst loadings (Figure 3a). The onset potential (E_{on}) was similar for Fe-ABZIM and Fe-BZIM independently from the loading and was quantified in +0.270 V (vs Ag/AgCl). Much lower onset potential was recorded for AC (−0.09 V (vs Ag/AgCl)). As expected, E_{on} was independent of the catalyst loading being a characteristic of intrinsic oxygen reduction reaction activity. Considering half-wave potential, at lower loading (0.1 mg cm^{-2}), Fe-BZIM had similar half-wave potential compared to Fe-ABZIM with a value of +0.126 ± 0.012 V (vs Ag/AgCl). At the same time AC had the lowest observed value (≈−0.270 V (vs Ag/AgCl)) (Figure 3a). The same trend in $E_{1/2}$ was recorded at higher loading (Figure 3a) however, Fe-BZIM has

a slightly higher electrocatalytic activity compared to Fe-ABZIM. Limiting currents with loading of 0.1 mg cm^{-2} were 3.3, 3.2, and 2.8 mA cm^{-2} for Fe-BZIM, Fe-ABZIM, and AC, respectively. The increase of catalyst loading on the working electrode resulted in significant increase of the limiting current achieving values of 5.5, 5.4, and 3.8 mA cm^{-2} for Fe-BZIM, Fe-ABZIM, and AC, respectively. On the basis of the analysis of RRDE data, it can be concluded that AC kinetics was very poor compared to Fe-based catalysts.

The hydrogen peroxide produced was also monitored by the ring current (I_{ring}) measured during the experiments (Figure 3b) and calculated through eq 1 considering the disk current (I_{disk}) and the collection efficiency of the ring ($N = 0.43$)

$$\%H_2O_2 = \frac{200 \times \frac{I_{ring}}{N}}{I_{disk} + \frac{I_{ring}}{N}} \tag{1}$$

Hydrogen peroxide yield was severely affected by the catalyst loading on the disk (Figure 3c). The increase in thickness decreased the production of peroxide, which is expected since a thicker catalyst layer tends to trap the intermediate within the layer itself and either further reduce it electrochemically or chemically decompose to water and oxygen. The AC had a peroxide yield of over 80% that decreased with the lower potentials scanned (Figure 3c). Fe-based catalysts had a very low peroxide yield produced, always lower than 3%, indicating a high efficiency toward complete 4e$^-$ ORR (Figure 3c). It also was observed in this case, that a thicker layer reduced the H_2O_2 yield produced.

The ORR can occur following a 2e$^-$, a direct 4e$^-$ or consecutive $2 \times 2e^-$ mechanism.[90,95] In a 4e$^-$ transfer mechanism, the ORR occurs on a single catalytic site with the complete conversion of the reactant into the final product (oxygen into the water). When a 2e$^-$ transfer mechanism occur, the intermediate can also be transformed chemically or electrochemically in the final product. The intermediate can, in fact, reacts on a secondary active site and is further reduced following a $2 \times 2e^-$ transfer mechanism. A direct 4e$^-$ is preferred compared to a 2e$^-$ since doubles number of electrons transferred for the same moles of oxygen reduced. Moreover, a direct 4e$^-$ transfer mechanism is also preferred and more efficient compared to a $2 \times 2e^-$ mechanism since a single catalytic site is used, and therefore, a faster conversion of oxygen into the final product is achieved (higher overall TOF). In this work, the number of electrons transferred was calculated according to eq 2

$$n = \frac{4 \times I_{disk}}{I_{disk} + \frac{I_{ring}}{N}} \tag{2}$$

Electron transfer number in the case of Fe-ABZIM and Fe-BZIM tends to match an "apparent" 4e$^-$ mechanism and shown in Figure 3d. At both loadings, in fact, the calculated

Table 1. Elemental Composition and Chemical Speciation of Fe-ABZIM and Fe-BZIM, As Evaluated by XPS Analysis

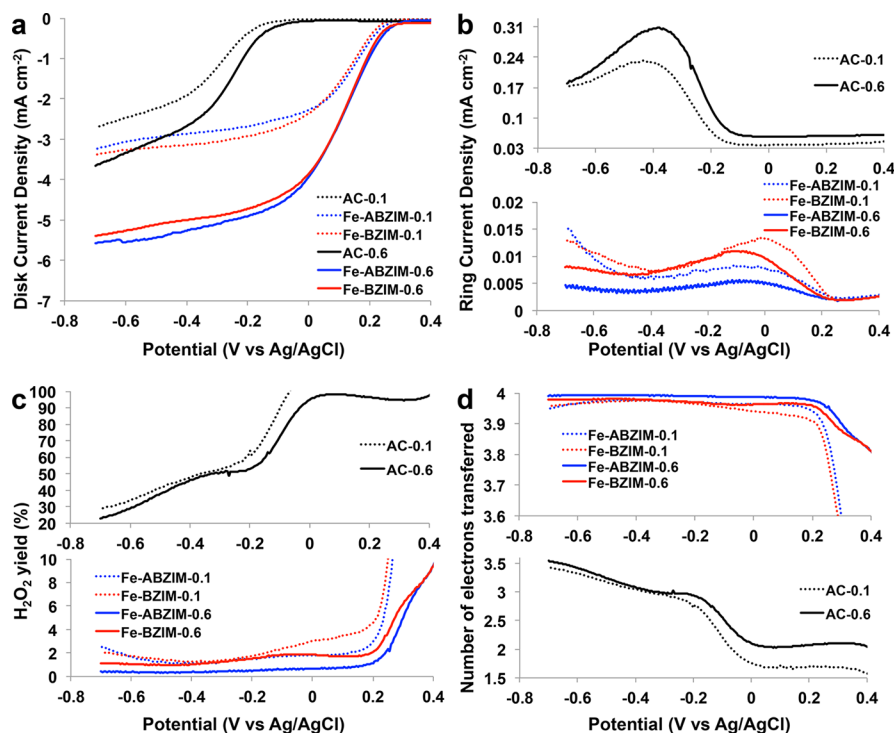|	C 1s (at. %)	O 1s (at. %)	N 1s (at. %)	Fe 2p (at. %)	C_{gr} (rel. %)	C* (rel. %)	C−N (rel. %)	C_xO_y (rel. %)
Fe-ABZIM	91	6	2.8	0.2	38.8	34	10.2	14.7
Fe-BZIM	90.4	6.7	2.8	0.1	38	33.4	13.1	14.1
	N imine (rel. %)	N pyr (rel. %)	N_x−Fe (rel. %)	N−H (rel. %)	N_{gr}/N^+ (rel. %)	NOx (rel. %)		
Fe-ABZIM	3.4	22.2	14.4	33.2	13	13.7		
Fe-BZIM	2.9	23.5	12.2	35.4	13.1	12.9		

Figure 3. Disk current (a), ring current (b), peroxide yield produced (c), and electron transfer number (d) of AC (black), Fe-BZIM (red), and Fe-ABZIM (blue) at two different Fe−N−C catalyst loading (0.1 and 0.6 mg cm^{-2}).

number is above 3.95. The study on the variation of loading was done to understand the influence of catalyst layer thickness on peroxide produced and therefore use that knowledge for prediction of the ORR mechanism. Despite very low peroxide yield in case of Fe-BZIM/Fe-ABZIM catalysts, the decrease of peroxide detected with the loading increased can be an indication of a 2 × 2e$^-$ mechanism. This observation is consistent with the previous RRDE studies done under similar operating conditions using M−N−C type of PGM-free catalysts for oxygen reduction reaction.[85,86,90−92] It was clearly shown in RRDE experiments that ORR on AC followed a 2 e$^-$ transfer mechanism which resulted in the highest amount of H$_2$O$_2$ produced (Figure 3c), while the number of electrons transferred is significantly lower than 3.5 (Figure 3d). The increase in loading decreased the hydrogen peroxide production and also increased significantly the number of electron transferred unambiguously supporting the explanation related to thicker layer trap of peroxide inside followed by its disproportionation before being oxidized on the ring.

3.3. Impedance Spectra of the Cathodes. To get deeper insights on the electrochemical behavior of the two types of cathodes in operating MFCs, cathodic EIS spectra at different current densities were acquired. Figure 4 showed the Nyquist plots under open circuit voltage (OCV) condition for Fe-BZIM-AB and Fe-BZIM-GDL cathodes. Both spectra showed a high-frequency process related to charge transfer (activation) at the cathode and a low-frequency process related to mass transfer limitations.[96] These plots were fitted using the equivalent electrical circuit that is illustrated in Figure 4. The latter consisted of ohmic resistance, in series with a Randles type circuit to model the high-frequency process, and with an additional Randles type circuit added by a Warburg diffusion element to model the low-frequency process associate to mass diffusion limitation.[97,98] In particular, R1 represents the ohmic
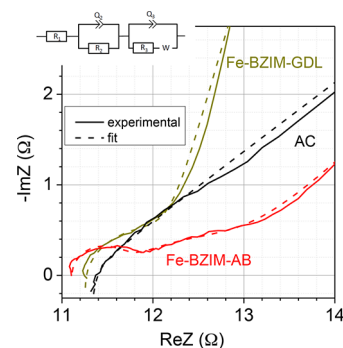

Figure 4. Nyquist plots under OCV condition ($J = 0$ mAm^{-2}) for Fe-BZIM and Fe-BZIM GDL cathodes. The equivalent circuit model is also reported in this figure.

resistance, Q2 a constant phase element associated with the double layer capacitance, R2 the charge transfer resistance (activation polarization), Q3 a constant phase element associated with the biofilm developed at the cathode, and R3 the mass transfer resistance (concentration polarization).

The fitting results of Nyquist plots for Fe-BZIM-AB, Fe-BZIM-GDL, and AC are shown in Table 2, indicating that (i) ohmic resistance (R1), because of the solution resistance, is similar for the three cathodes and that (ii) mass transport resistance (R3) is similar for bare AC and Fe-BZIM-AB, while

Table 2. Fitting Results of Nyquist Plots for Fe-BZIM-AB and Fe-BZIM-GDL Electrodes

cathode	R1 (Ω)	R2 (Ω)	R3 (Ω)
Fe-BZIM-AB	11.1 ± 0.1	0.91 ± 0.01	1.08 ± 0.95
Fe-BZIM-GDL	11.2 ± 0.2	1.43 ± 0.09	29.40 ± 2.30
AC	11.3 ± 0.2	1.89 ± 0.15	1.23 ± 0.91

it is much higher for Fe-BZIM-GDL. This behavior can be ascribed to the higher PTFE loading of GDL cathodes as compared to AB-cathodes that hinders oxygen diffusion with respect to air-breathing cathodes resulting in mass transport losses. Also, in the case of GDL cathodes, PTFE layers at the air-side further contributing to the high mass transport resistance of GDL cathodes. Catalyst flooding can also explain the higher charge transfer (R2) resistance of Fe-BZIM-GDL that that of Fe-BZIM-AB, (iii) as expected, bare AC has higher charge transfer resistance than that of Fe-BZIM-AB due to the beneficial effect of the catalyst in reducing activation losses.

3.4. Initial Performance in Operating MFC. After the determination of the catalyst kinetics by RRDE method, these materials were incorporated into the air-breathing (AB) and gas diffusional layer (GDL) cathodes, followed by MFC testing. MFCs with Fe-based cathodes had similar OCV of 0.68 ± 0.03 V. Slightly lower was the OCV measured with the MFC with the AC-based cathode (Figure 5a). The polarization
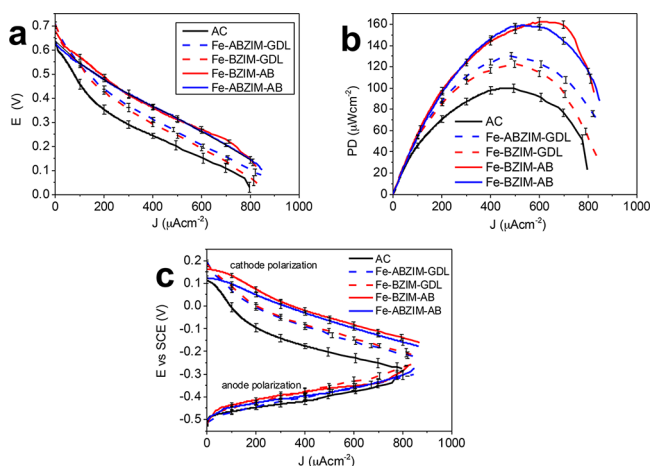

Figure 5. MFCs polarization curves obtained with different cathodes (a), power curves (b), and anode−cathode polarization curves (c).

curves can be ascribed as straight lines indicating that the MFCs were mainly subject to the ohmic behavior agrees with previously presented data.[85,90,91] The MFCs with AB cathodes containing Fe−N−C catalysts outperformed compared to the GDL cathodes containing Fe−N−C. The AC-based cathodes MFCs were the lowest performing (Figure 5a). Interestingly, the method of cathode fabrication had a higher effect on the fuel cell performance compared with the influence of catalyst type (Fe-BZIM vs Fe-ABZIM) when last had similar performance. The power densities generated by these types of MFCs are shown in Figure 5b. The maximal power density was obtained in the case of MFC contained Fe-BZIM-AB cathode (162 ± 3 μW m^{-2}) followed by Fe-ABZIM with very similar performance (159 ± 3 μW m^{-2}). GDL type MFCs had systematically lower performance compared with AB-type of electrodes reaching only 130 ± 2 (Fe-ABZIM-GDL) and 122 ± 2 μW m^{-2} (Fe-BZIM-GDL). The lowest performance was measured in case of an AC-based cathode having 100 ± 3 μW m^{-2}. The use of AB-type cathode compared to GDL-type resulted in 33% of power density for Fe-BZIM and 23% in the case of Fe-ABZIM catalyst. The best performing MFCs with AB-type and GDL-type cathodes had a power output that was 63% and 30% higher than AC-cathode MFC.

The main difference in the overall MFC performance was caused by the cathode behavior as enhanced by the cathode

polarization profile showed in Figure 5c. Interestingly, the anode polarization performed similarly for all the MFCs investigated, confirming the idea that ORR is mainly responsible for performance losses (Figure 5c). Once incorporated in either AB or GDL cathodes, Fe-ABZIM- and Fe-BZIM-based catalysts performed similarly (Figure 5c). The comparison of the two types of cathodes highlights that OCV values of GDL cathodes are higher than the one achieved by the AB cathodes. By contrast, as the current density increases the AB cathodes outperform the GDL ones. The lower ohmic and charge-transfer resistance of AB cathodes described in section 3.3, is reflected on the cathode polarization curves and consequently on the overall cell polarization and power density generation (Figure 5 and Table 3).

Table 3. OCV Values, Current Density at 0.3 V, and Peak Power Density (PD) Measured for the MFC Systems

cathode	OCV (V)	J@0.3 V (μA cm^{-2})	PD$_{peak}$ (μW cm^{-2})
Fe-BZIM-AB	0.68 ± 0.01	529 ± 8	162 ± 4
Fe-BZIM-GDL	0.70 ± 0.01	382 ± 7	122 ± 3
Fe-ABZIM-AB	0.64 ± 0.01	529 ± 8	159 ± 3
Fe-ABZIM-GDL	0.71 ± 0.01	418 ± 7	130 ± 4
AC	0.62 ± 0.02	281 ± 4	100 ± 4

3.5. Long-Term Durability Study. Long-term durability of two types of cathodes was also evaluated by acquiring voltage generation cycles over time under 1 kΩ external load (Figure 6). It can be seen that all the MFCs had stable voltage over roughly 60 days (Figure 6).
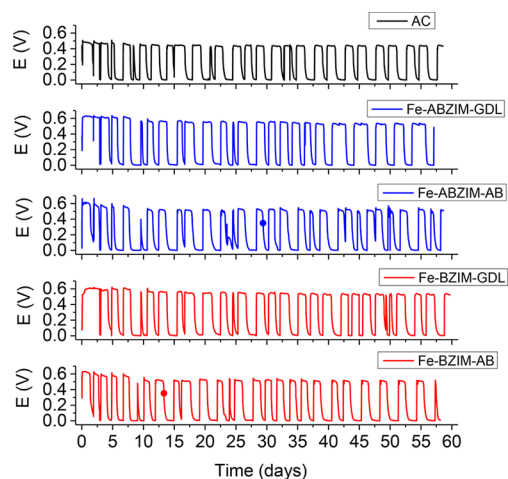

Figure 6. Voltage generation cycles under a 1 kΩ over 60 days from beginning of experiment (BoE) values.

In a parallel, the durability of two types of cathodes was evaluated by monitoring produced peak power density (PD$_{peak}$) (Figure 7). As a general trend, PD$_{peak}$ for reference AC cathode sharply decreases after 7 days of operation following by continuous degradation, finally reaching 50% of the original value after 50 days. The PD$_{peak}$ refers to a high current density regime (>3−4 A m^{-2}), and the decrease can be attributed to ohmic losses and mass transfer limitations which increase over time due to biofilm formation and salts precipitation on the cathode interfaces (rather than catalyst deactivation). Salts precipitation and biofilm formation affect
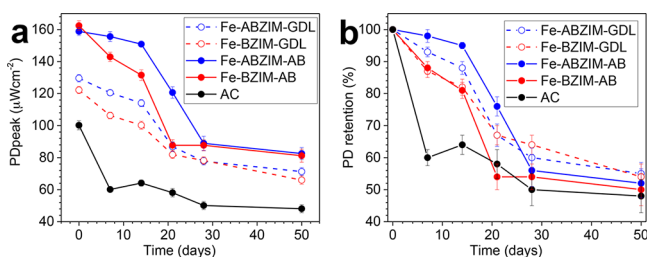
Figure 7. (a) Peak PD retention and (b) peak PD over the time for the MFC cells assembled with pristine AC and Fe−N−C cathodes.

significantly the power output resulting in its significant decrease over the time as it was previously presented.[99−103]

On the other hand, the catalysts enhanced the PD_{peak} as compared to reference AC. In particular, for Fe-based cathodes, PD_{peak} decreases very slightly during the first 2 weeks of operations ($\approx 142 \pm 10$ and $\approx 107 \pm 7$ μW cm^{-2} for AB and GDL types, respectively (Figure 7.a)). It should be mentioned that AC had a decrease in PD_{peak} of 40% ($\approx 60 \pm 2$ μW cm^{-2}) within 7 days operations and then remained approximately stable over the remaining 40 days with PD_{peak} of $\approx 50 \pm 2$ μW cm^{-2} after 50 days. A lost in PD_{peak} quantified in more than 40% of the original value was evaluated after one month of operation. After that, PD_{peak} remains stable up to 50 days for Fe-based-AB while slightly decreased for Fe-based-GDL (Figure 7). After 50 days, Fe-based-AB had a PD_{peak} of 81 ± 4 μW cm^{-2}, while Fe-based-GDL had a power peak of 69 ± 2 μW cm^{-2} (Figure 7). Fe-based catalyst after 50 days still had an advantage of 62% and 38% compared to AC when operating in AB or GDL mode, respectively (Figure 7).

4. DISCUSSION AND COMPARISON WITH EXISTING LITERATURE

Two different Fe−N−C electrocatalysts were prepared using sacrificial support method (SSM). Highly rich in nitrogen and carbon organic precursors benzimidazole (BZIM) and amino-benzimidazole (ABZIM) were used as an N−C matrix. The formation of ORR active sites was achieved by the addition of iron, while using silica as a hard template allowed to increase the density of active sites. The process produced catalysts with atomically dispersed iron, as well as with a 3D morphological structure having characteristic porosity formed after a silica etching and during the organic precursor decomposition. Moreover, the pyrolysis process created a material rich in nitrogen with pyridinic nitrogen as the most desired and present defect nitrogen form. Fe-BZIM and Fe-ABZIM had similar surface chemistry which in this case is also somehow expected due to similar organic precursors utilized. The two catalysts also have high electrocatalytic activity in RRDE with low, but still not negligible; peroxide produced indicating that these materials are quite efficient toward the reduction of oxygen in neutral media. The variation of peroxide production with the loading underlined a probable $2 \times 2e^-$ transfer mechanism. AC, used as a control, showed to have a direct $2e^-$ transfer mechanism and high peroxide production in agreement with previously presented works.[85,86,90−92]

The catalysts were then integrated into different cathode structures. The first one named air-breathing (AB) cathode had the catalyst mixed within the AC/PTFE/CB matrix before being pressed on the current collector. The second one, named gas diffusion layer (GDL), was composed of the mixture AC/PTFE/CB pressed over the current collector. Once the pellet

was formed, the catalyst was sprayed on the internal cathode part. AC/PTFE/CB with no addition of any Fe-based catalyst was used as a control. Performance in MFCs showed that AB-type cathode outperformed GDL-type cathode. This result was also confirmed by the EIS tests in which AB-cathode had lower ohmic and charge transfer resistance compared to GDL-cathode. The better water management of the AB-type with a probable clear three-phase interface (TPI) formed might also be another explanation supporting the better performance with GDL-cathode catalyst fully flooded and therefore with lower power output. Fe-BZIM and Fe-ABZIM had similar performance when used in the same cathode structure. In operating MFCs, Fe-based cathode outperformed significantly the AC used as a control. The highest power generated in this study was 162 ± 3 μW cm^{-2} achieved by Fe-BZIM-AB, and the GDL type cathode achieved a maximum power density of 130 ± 2 μW cm^{-2} (Fe-ABZIM-GDL). AC had a maximum power density of 100 ± 3 $\mu W cm^{-2}$. The present work not only shown the advancement in performance due to the utilization of Fe-based catalysts compared to bare AC but it also indicates, which type of cathode structure should be used for optimizing the electrochemical output.

Several works were presented previously considering Fe-based materials as ORR catalysts, but a direct comparison of their activity is quite complicated because of the difference in operating conditions such as working temperature, electrolyte solution conductivity, MFC design, catalyst loading and a different number of anode brushes used. Moreover, the pH of the electrolyte affects the cathodic electrochemical performance and reaction mechanism significantly.[90] It was shown previously that the increase in temperature has a positive effect on the anode electrokinetics that gave a considerable advantage to the overall performance.[104,105] The highest power density (expressed in function of the cathode geometric area) presented in the literature using (i) similar electrolyte composition; (ii) diverse Fe-based cathodes catalyst and loading; and (iii) similar MFC configuration but operating at a constant temperature of 30 °C were able to achieve the value of roughly 278 μW cm^{-2}.[106] This present work was conducted at room temperature with penalized anode performance. The higher operating temperature was shown to be beneficial for the anode performance improving the overall performance.[104,105] Existing literature on Fe-based cathode materials with the catalyst synthesized using SSM technique generated a power density that varied between 167 and 235 μW cm^{-2} considering the same catalyst loading and identical operating temperature.[30,31,59,77,85,86,91,92] The performance here reported are slightly lower, and this is mainly due to the utilization of (i) an electrolyte with lower solution conductivity and (ii) a single brush rather the two as an anode. It was shown that solution conductivity affects dramatically the power output.[85,87] Moreover, comparing the anode polarization curve here measured and the one identified in a previous research,[77] it can be seen the utilization of a single brush MFC rather than the double brush lead to a lower output penalizing the overall output. Interestingly, the power density reported using Fe-based catalyst is superior compared to Co-based, Mn-based, and Ni-based catalysts in agreement with standing state of the art literature.[85,86] In contrast, different behavior is observed with Mn-based oxides outperforming Fe-based oxides and showing higher durability at long terms operations.[107]

Durability tests presented show degradation in PD_{peak} up to 50% after roughly 30 days of operation. This is in disagreement

with previously presented literature in which the decrease in output with time was less evidenced and quantified in 20−40% over a longer period. Usually the decrease in electrochemical output is associated with the presence of inorganic or biological fouling that might (i) accelerate poisoning, interact or deactivate the catalytic sites; (ii) block and clog the pores within the cathode structure reducing the oxygen to reach the catalytic sites; (iii) consume the oxygen before reaching the catalytic site; (iv) create a carbonate layer that increase the mass transfer resistance of protons from the electrolyte to reach the catalytic sites. Efficient in situ removal of the biofilm from an air-breathing cathode have been recently proposed.[108] All those three possibilities might have happened in this study, and further investigations are certainly needed to enhance the understanding of these processes and insert procedures to avoid fouling and this drastic loss in performance.

5. CONCLUSIONS

A new set of catalyst was synthesized using the sacrificial support method technique. Benzimidazole (BZIM) and aminobenzimidazole (ABZIM) were used as organic nitrogen rich precursor and mixed within iron salt during the high-temperature treatment. Silica template was then etched after pyrolysis creating a well-defined 3D catalyst structure. The catalysts showed much higher electrocatalytic activity toward oxygen reduction reaction in neutral media compared to activated carbon (AC) used as a baseline. The catalysts were then integrated into two diverse types of cathodes: gas diffusion layer (GDL) and air-breathing (AB). Tests in operating MFCs showed that the higher performance were achieved in the AB type with a maximum recorded of 162 ± 3 μWcm^{-2}. The results suggest utilizing a Fe-based catalyst to enhance the power output of MFCs. Moreover, also the cathode structure had an important effect on the power output with the air-breathing configuration as the most suitable for higher performance.

■ AUTHOR INFORMATION

Corresponding Authors
*E-mail: barbara.mecheri@uniroma2.it. Phone: +39 06 7259 4488.
*E-mail: santoro@unm.edu. Phone: +1 505 277 2640.
ORCID
Barbara Mecheri: 0000-0002-1458-6239
Carlo Santoro: 0000-0002-0944-4500
Kateryna Artyushkova: 0000-0002-2611-0422
Plamen Atanassov: 0000-0003-2996-472X
Notes
The authors declare no competing financial interest.

■ REFERENCES

(1) Rinaldi, A.; Mecheri, B.; Garavaglia, V.; Licoccia, S.; Di Nardo, P.; Traversa, E. Engineering materials and biology to boost performance of microbial fuel cells: a critical review. *Energy Environ. Sci.* **2008**, *1*, 417−429.

(2) Santoro, C.; Arbizzani, C.; Erable, B.; Ieropoulos, I. Microbial fuel cells: from fundamentals to applications. A review. *J. Power Sources* **2017**, *356*, 225−244.

(3) Pandey, P.; Shinde, V. N.; Deopurkar, R. L.; Kale, S. P.; Patil, S. A.; Pant, D. Recent advances in the use of different substrates in microbial fuel cells toward wastewater treatment and simultaneous energy recovery. *Appl. Energy* **2016**, *168*, 706−723.

(4) Bajracharya, S.; Srikanth, S.; Mohanakrishna, G.; Zacharia, R.; Strik, D. P.; Pant, D. Biotransformation of carbon dioxide in bioelectrochemical systems: State of the art and future prospects. *J. Power Sources* **2017**, *356*, 256−273.

(5) Rimboud, M.; Desmond-Le Quemener, E.; Erable, B.; Bouchez, T.; Bergel, A. The current provided by oxygen-reducing microbial cathodes is related to the composition of their bacterial community. *Bioelectrochemistry* **2015**, *102*, 42−49.

(6) Doyle, L. E.; Yung, P. Y.; Mitra, S. D.; Wuertz, S.; Williams, R. B. H.; Lauro, F. M.; Marsili, E. Electrochemical and genomic analysis of novel electroactive isolates obtained via potentiostatic enrichment from tropical sediment. *J. Power Sources* **2017**, *356*, 539−548.

(7) Kumar, A.; Hsu, L. H. H.; Kavanagh, P.; Barrière, F.; Lens, P. N. L.; Lapinsonnière, L.; Lienhard, J. H., V; Schröder, U.; Jiang, X.; Leech, D. The ins and outs of microorganism−electrode electron transfer reactions. *Nat. Rev. Chem.* **2017**, *1*, 24.

(8) Ucar, D.; Zhang, Y.; Angelidaki, I. An Overview of Electron Acceptors in Microbial Fuel Cells. *Front. Microbiol.* **2017**, *8*, 643.

(9) Schievano, A.; Colombo, A.; Grattieri, M.; Trasatti, S. P.; Liberale, A.; Tremolada, P.; Pino, C.; Cristiani, P. Floating microbial fuel cells as energy harvesters for signal transmission from natural water bodies. *J. Power Sources* **2017**, *340*, 80−88.

(10) Walter, X. A.; Merino-Jiménez, I.; Greenman, J.; Ieropoulos, I. PEE POWER® urinal II − Urinal scale-up with microbial fuel cell scale-down for improved lighting. *J. Power Sources* **2018**, *392*, 150−158.

(11) Arias-Thode, Y. M.; Hsu, L.; Anderson, G.; Babauta, J.; Fransham, R.; Obraztsova, A.; Tukeman, G.; Chadwick, D. B. Demonstration of the SeptiStrand benthic microbial fuel cell powering a magnetometer for ship detection. *J. Power Sources* **2017**, *356*, 419−429.

(12) Lu, M.; Chen, S.; Babanova, S.; Phadke, S.; Salvacion, M.; Mirhosseini, A.; Chan, S.; Carpenter, K.; Cortese, R.; Bretschger, O. Long-term performance of a 20-L continuous flow microbial fuel cell for treatment of brewery wastewater. *J. Power Sources* **2017**, *356*, 274−287.

(13) Rismani-Yazdi, H.; Carver, S. M.; Christy, A. D.; Tuovinen, O. H. Cathodic limitations in microbial fuel cells: An overview. *J. Power Sources* **2008**, *180*, 683−694.

(14) Madjarov, J.; Popat, S. C.; Erben, J.; Götze, A.; Zengerle, R.; Kerzenmacher, S. Revisiting methods to characterize bioelectrochemical systems: The influence of uncompensated resistance (iRu-drop), double layer capacitance, and junction potential. *J. Power Sources* **2017**, *356*, 408−418.

(15) Kinoshita, K. *Carbon: Electrochemical and Physicochemical Properties*; John Wiley Sons: New York, NY, 1988.

(16) Kinoshita, K. *Electrochemical Oxygen Technology*; John Wiley Sons: New York, NY, 1992.

(17) Erable, B.; Feron, D.; Bergel, A. Microbial catalysis of the oxygen reduction reaction for microbial fuel cells: a review. *ChemSusChem* **2012**, *5*, 975−987.

(18) Huang, L.; Regan, J. M.; Quan, X. Electron transfer mechanisms, new applications, and performance of biocathode microbial fuel cells. *Bioresour. Technol.* **2011**, *102*, 316−323.

(19) Rago, L.; Cristiani, P.; Villa, F.; Zecchin, S.; Colombo, A.; Cavalca, L.; Schievano, A. Influences of dissolved oxygen concentration on biocathodic microbial communities in microbial fuel cells. *Bioelectrochemistry* **2017**, *116*, 39−51.

(20) Atanassov, P.; Apblett, C.; Banta, S.; Brozik, S.; Barton, S. C.; Cooney, M.; Liaw, B. Y.; Mukerjee, S.; Minteer, S. D. Enzymatic biofuel cells. *Electrochem. Soc. Interface* **2007**, *16*, 28−31.

(21) Falk, M.; Narváez Villarrubia, C. W.; Babanova, S.; Atanassov, P.; Shleev, S. Biofuel Cells for Biomedical Applications: Colonizing the Animal Kingdom. *ChemPhysChem* **2013**, *14*, 2045−2058.

(22) Rasmussen, M.; Abdellaoui, S.; Minteer, S. D. Enzymatic biofuel cells: 30 years of critical advancements. *Biosens. Bioelectron.* **2016**, *76*, 91−102.

(23) Cooney, M. J.; Svoboda, V.; Lau, C.; Martin, G.; Minteer, S. D. Enzyme catalysed biofuel cells. *Energy Environ. Sci.* **2008**, *1*, 320−337.

(24) Mano, N.; de Poulpiquet, A. O$_2$ Reduction in Enzymatic Biofuel Cells. *Chem. Rev.* **2018**, *118*, 2392−2468.

(25) Santoro, C.; Babanova, S.; Erable, B.; Schuler, A.; Atanassov, P. Bilirubin oxidase based enzymatic air-breathing cathode: Operation under pristine and contaminated conditions. *Bioelectrochemistry* **2016**, *108*, 1−7.

(26) Oliot, M.; Etcheverry, L.; Mosdale, A.; Basseguy, R.; Delia, M.-L.; Bergel, A. Separator electrode assembly (SEA) with 3-dimensional bioanode and removable air-cathode boosts microbial fuel cell performance. *J. Power Sources* **2017**, *356*, 389−399.

(27) Antolini, E. Composite materials for polymer electrolyte membrane microbial fuel cells. *Biosens. Bioelectron.* **2015**, *69*, 54−70.

(28) Yuan, H.; Hou, Y.; Abu-Reesh, I. M.; Chen, J.; He, Z. Oxygen reduction reaction catalysts used in microbial fuel cells for energy-efficient wastewater treatment: a review. *Mater. Horiz.* **2016**, *3*, 382−401.

(29) Wang, Z.; Cao, C.; Zheng, Y.; Chen, S.; Zhao, F. Abiotic Oxygen Reduction Reaction Catalysts Used in Microbial Fuel Cells. *ChemElectroChem* **2014**, *1*, 1813−1821.

(30) Santoro, C.; Serov, A.; Narvaez Villarrubia, C. W.; Stariha, S.; Babanova, S.; Artyushkova, K.; Schuler, A. J.; Atanassov, P. High catalytic activity and pollutants resistivity using Fe-AAPyr cathode catalyst for microbial fuel cell application. *Sci. Rep.* **2015**, *5*, 16596.

(31) Santoro, C.; Serov, A.; Stariha, L.; Kodali, M.; Gordon, J.; Babanova, S.; Bretschger, O.; Artyushkova, K.; Atanassov, P. Iron based catalysts from novel low-cost organic precursors for enhanced oxygen reduction reaction in neutral media microbial fuel cells. *Energy Environ. Sci.* **2016**, *9*, 2346−2353.

(32) Santoro, C.; Rezaei Talarposhti, M.; Kodali, M.; Gokhale, R.; Serov, A.; Merino- Jimenez, I.; Ieropoulos, I.; Atanassov, P. Microbial Desalination Cells with Efficient Platinum-Group-Metal-Free Cathode Catalysts. *ChemElectroChem* **2017**, *4*, 3322−3330.

(33) Arbizzani, C.; Beninati, S.; Soavi, F.; Varzi, A.; Mastragostino, M. Supported PtRu on mesoporous carbons for direct methanol fuel cells. *J. Power Sources* **2008**, *185*, 615−620.

(34) Yu, X.; Ye, S. Recent advances in activity and durability enhancement of Pt/C catalytic cathode in PEMFC: Part II: Degradation mechanism and durability enhancement of carbon supported platinum catalyst. *J. Power Sources* **2007**, *172*, 145−154.

(35) Mustakeem. Electrode materials for microbial fuel cells: nanomaterial approach. *Mater. Renew. Sustain. Energy* **2015**, *4*, 22.

(36) Guo, K.; Prevoteau, A.; Patil, S. A.; Rabaey, K. Engineering electrodes for microbial electrocatalysis. *Curr. Opin. Biotechnol.* **2015**, *33*, 149−156.

(37) Wei, J.; Liang, P.; Huang, X. Recent progress in electrodes for microbial fuel cells. *Bioresour. Technol.* **2011**, *102*, 9335−9344.

(38) Grattieri, M.; Suvira, M.; Hasan, K.; Minteer, S. D. Halotolerant extremophile bacteria from the Great Salt Lake for recycling pollutants in microbial fuel cells. *J. Power Sources* **2017**, *356*, 310−318.

(39) Grattieri, M.; Shivel, N. D.; Sifat, I.; Bestetti, M.; Minteer, S. D. Sustainable Hypersaline Microbial Fuel Cells: Inexpensive Recyclable Polymer Supports for Carbon Nanotube Conductive Paint Anodes. *ChemSusChem* **2017**, *10*, 2053−2058.

(40) Karra, U.; Muto, E.; Umaz, R.; Kolln, M.; Santoro, C.; Wang, L.; Li, B. Performance evaluation of activated carbon-based electrodes with novel power management system for long-term benthic microbial fuel cells. *Int. J. Hydrogen Energy* **2014**, *39*, 21847−21856.

(41) Dong, H.; Yu, H.; Yu, H.; Gao, N.; Wang, X. Enhanced performance of activated carbon−polytetrafluoroethylene air-cathode by avoidance of sintering on catalyst layer in microbial fuel cells. *J. Power Sources* **2013**, *232*, 132−138.

(42) Gajda, I.; Greenman, J.; Melhuish, C.; Ieropoulos, I. Simultaneous electricity generation and microbially-assisted electro-synthesis in ceramic MFCs. *Bioelectrochemistry* **2015**, *104*, 58−64.

(43) Zhang, F.; Pant, D.; Logan, B. E. Long-term performance of activated carbon air cathodes with different diffusion layer porosities in microbial fuel cells. *Biosens. Bioelectron.* **2011**, *30*, 49−55.

(44) Sevda, S.; Dominguez-Benetton, X.; Vanbroekhoven, K.; De Wever, H.; Sreekrishnan, T. R.; Pant, D. High strength wastewater treatment accompanied by power generation using air cathode microbial fuel cell. *Appl. Energy* **2013**, *105*, 194−206.

(45) Soavi, F.; Bettini, L. G.; Piseri, P.; Milani, P.; Santoro, C.; Atanassov, P.; Arbizzani, C. Miniaturized supercapacitors: key materials and structures towards autonomous and sustainable devices and systems. *J. Power Sources* **2016**, *326*, 717−725.

(46) Merino-Jimenez, I.; Santoro, C.; Rojas-Carbonell, S.; Greenman, J.; Ieropoulos, I.; Atanassov, P. Carbon-based air-breathing cathodes for microbial fuel cells. *Catalysts* **2016**, *6*, 127.

(47) Zhang, X.; He, W.; Zhang, R.; Wang, Q.; Liang, P.; Huang, X.; Logan, B. E.; Fellinger, T.-P. High-Performance Carbon Aerogel Air Cathodes for Microbial Fuel Cells. *ChemSusChem* **2016**, *9*, 2788−2795.

(48) Wang, H.; Wu, Z.; Plaseied, A.; Jenkins, P.; Simpson, L.; Engtrakul, C.; Ren, Z. Carbon nanotube modified air-cathodes for electricity production in microbial fuel cells. *J. Power Sources* **2011**, *196*, 7465−7469.

(49) Ghasemi, M.; Shahgaldi, S.; Ismail, M.; Kim, B. H.; Yaakob, Z.; Wan Daud, W. R. Activated carbon nanofibers as an alternative cathode catalyst to platinum in a two-chamber microbial fuel cell. *Int. J. Hydrogen Energy* **2011**, *36*, 13746−13752.

(50) Wang, Q.; Zhang, X.; Lv, R.; Chen, X.; Xue, B.; Liang, P.; Huang, X. Binder-free nitrogen-doped graphene catalyst air-cathodes for microbial fuel cells. *J. Mater. Chem. A* **2016**, *4*, 12387−12391.

(51) Yuan, H.; He, Z. Graphene-modified electrodes for enhancing the performance of microbial fuel cells. *Nanoscale* **2015**, *7*, 7022−7029.

(52) Santoro, C.; Kodali, M.; Kabir, S.; Soavi, F.; Serov, A.; Atanassov, P. Three-dimensional graphene nanosheets as cathode catalysts in standard and supercapacitive microbial fuel cell. *J. Power Sources* **2017**, *356*, 371−380.

(53) Xiao, L.; Damien, J.; Luo, J.; Jang, H. D.; Huang, J.; He, Z. Crumpled graphene particles for microbial fuel cell electrodes. *J. Power Sources* **2012**, *208*, 187−192.

(54) Wang, Z.; Mahadevan, G. D.; Wu, Y.; Zhao, F. Progress of air-breathing cathode in microbial fuel cells. *J. Power Sources* **2017**, *356*, 245−255.

(55) Zhao, F.; Harnisch, F.; Schröder, U.; Scholz, F.; Bogdanoff, P.; Herrmann, I. Application of pyrolysed iron (II) phthalocyanine and CoTMPP based oxygen reduction catalysts as cathode materials in microbial fuel cells. *Electrochem. Commun.* **2005**, *7*, 1405−1410.

(56) Zhao, F.; Harnisch, F.; Schröder, U.; Scholz, F.; Bogdanoff, P.; Herrmann, I. Challenges and constraints of using oxygen cathodes in microbial fuel cells. *Environ. Sci. Technol.* **2006**, *40*, 5193−5199.

(57) Costa de Oliveira, M. A.; Mecheri, B.; D'Epifanio, A.; Placidi, E.; Arciprete, F.; Valentini, F.; Perandini, A.; Valentini, V.; Licoccia, S. Graphene oxide nanoplatforms to enhance catalytic performance of iron phthalocyanine for oxygen reduction reaction in bioelectrochemical systems. *J. Power Sources* **2017**, *356*, 381−388.

(58) Burkitt, R.; Whiffen, T. R.; Yu, E. H. Iron phthalocyanine and MnOx composite catalysts for microbial fuel cell applications. *Appl. Catal., B* **2016**, *181*, 279−288.

(59) Santoro, C.; Gokhale, R.; Mecheri, B.; D'Epifanio, A.; Licoccia, S.; Serov, A.; Artyushkova, K.; Atanassov, P. Design of Iron(II) Phthalocyanine-Derived Oxygen Reduction Electrocatalysts for High-Power-Density Microbial Fuel Cells. *ChemSusChem* **2017**, *10*, 3243−3251.

(60) Serov, A. A.; Min, M.; Chai, G.; Han, S.; Seo, S. J.; Park, Y.; Kim, H.; Kwak, C. Electroreduction of oxygen over iron macrocyclic catalysts for DMFC applications. *J. Appl. Electrochem.* **2009**, *39*, 1509−1516.

(61) Sebastián, D.; Serov, A.; Artyushkova, K.; Gordon, J.; Atanassov, P.; Arico, A. S.; Baglio, V. High Performance and Cost-Effective Direct Methanol Fuel Cells: Fe-N-C Methanol-Tolerant Oxygen Reduction Reaction Catalysts. *ChemSusChem* **2016**, *9*, 1986−1995.

(62) Reshetenko, T.; Serov, A.; Artyushkova, K.; Matanovic, I.; Stariha, S.; Atanassov, P. Tolerance of non-platinum group metals cathodes proton exchange membrane fuel cells to air contaminants. *J. Power Sources* **2016**, *324*, 556−571.

(63) Goellner, V.; Armel, V.; Zitolo, A.; Fonda, E.; Jaouen, F. Degradation by Hydrogen Peroxide of Metal-Nitrogen-Carbon Catalysts for Oxygen Reduction. *J. Electrochem. Soc.* **2015**, *162*, H403−H414.

(64) Negro, E.; Di Noto, V. Polymer electrolyte fuel cells based on bimetallic carbon nitride electrocatalysts. *J. Power Sources* **2008**, *178*, 634−641.

(65) Di Noto, V.; Negro, E. Synthesis, characterization and electrochemical performance of tri-metal Pt-free carbon nitride electrocatalysts for the oxygen reduction reaction. *Electrochim. Acta* **2010**, *55*, 1407−1418.

(66) Jiang, B.; Muddemann, T.; Kunz, U.; Bormann, H.; Niedermeiser, M.; Haupt, D.; Schlaefer, O.; Sievers, M. Evaluation of Microbial Fuel Cells with Graphite Plus MnO_2 and MoS_2 Paints as Oxygen Reduction Cathode Catalyst. *J. Electrochem. Soc.* **2017**, *164*, H3083−H3090.

(67) Li, X.; Hu, B.; Suib, S.; Lei, Y.; Li, B. Manganese dioxide as a new cathode catalyst in microbial fuel cells. *J. Power Sources* **2010**, *195*, 2586−2591.

(68) Shahbazi Farahani, F.; Mecheri, B.; Reza Majidi, M. R.; Costa de Oliveira, M. A.; D'Epifanio, A.; Zurlo, F.; Placidi, E.; Arciprete, F.; Licoccia, S. MnOx-based electrocatalysts for enhanced oxygen reduction in microbial fuel cell air cathodes. *J. Power Sources* **2018**, *390*, 45−53.

(69) Santoro, C.; Rojas-Carbonell, S.; Awais, R.; Gokhale, R.; Kodali, M.; Serov, A.; Artyushkova, K.; Atanassov, P. Influence of platinum group metal-free catalyst synthesis on microbial fuel cell performance. *J. Power Sources* **2018**, *375*, 11−20.

(70) Nguyen, M.-T.; Mecheri, B.; Iannaci, A.; D'Epifanio, A.; Licoccia, S. Iron/Polyindole-based Electrocatalysts to Enhance Oxygen Reduction in Microbial Fuel Cells. *Electrochim. Acta* **2016**, *190*, 388−395.

(71) Lu, G.; Zhu, Y.; Lu, L.; Xu, K.; Wang, H.; Jin, Y.; Ren, Z. J.; Liu, Z.; Zhang, W. Iron-rich nanoparticle encapsulated, nitrogen doped porous carbon materials as efficient cathode electrocatalyst for microbial fuel cells. *J. Power Sources* **2016**, *315*, 302−307.

(72) Santoro, C.; Serov, A.; Gokhale, R.; Rojas Carbonell, S.; Stariha, S.; Gordon, J.; Artyushkova, K.; Atanassov, P. A family of Fe-N-C oxygen reduction electrocatalysts for microbial fuel cell (MFC) application: Relationships between surface chemistry and performances. *Appl. Catal., B* **2017**, *205*, 24−33.

(73) Birry, L.; Mehta, P.; Jaouen, F.; Dodelet, J.-P.; Guiot, S. R.; Tartakovsky, B. Application of iron-based cathode catalysts in a microbial fuel cell. *Electrochim. Acta* **2011**, *56*, 1505−1511.

(74) Iannaci, A.; Mecheri, B.; D'Epifanio, A.; Lazaro Elorri, M. J.; Licoccia, S. Iron−nitrogen-functionalized carbon as efficient oxygen reduction reaction electrocatalyst in microbial fuel cells. *Int. J. Hydrogen Energy* **2016**, *41*, 19637−19644.

(75) Nguyen, M.-T.; Mecheri, B.; D'Epifanio, A.; Sciarria, T. P.; Adani, F.; Licoccia, S. Iron chelates as low-cost and effective electrocatalyst for oxygen reduction reaction in microbial fuel cells. *Int. J. Hydrogen Energy* **2014**, *39*, 6462−6469.

(76) Kodali, M.; Gokhale, R.; Santoro, C.; Serov, A.; Artyushkova, K.; Atanassov, P. High Performance Platinum Group Metal-Free Cathode Catalysts for Microbial Fuel Cell (MFC). *J. Electrochem. Soc.* **2017**, *164*, H3041−H3046.

(77) Kodali, M.; Santoro, C.; Herrera, S.; Serov, A.; Atanassov, P. Bimetallic platinum group metal-free catalysts for high power generating microbial fuel cells. *J. Power Sources* **2017**, *366*, 18−26.

(78) Hou, Y.; Yuan, H.; Wen, Z.; Cui, S.; Guo, X.; He, Z.; Chen, J. Nitrogen-doped graphene/CoNi alloy encased within bamboo-like carbon nanotube hybrids as cathode catalysts in microbial fuel cells. *J. Power Sources* **2016**, *307*, 561−568.

(79) Kumar, R.; Singh, L.; Zularisam, A. W.; Hai, F. I. Potential of porous Co_3O_4 nanorods as cathode catalyst for oxygen reduction reaction in microbial fuel cells. *Bioresour. Technol.* **2016**, *220*, 537−542.

(80) Yu, E. H.; Cheng, S.; Scott, K.; Logan, B. E. Microbial fuel cell performance with non-Pt cathode catalysts. *J. Power Sources* **2007**, *171*, 275−281.

(81) Huang, J.; Zhu, N.; Yang, T.; Zhang, T.; Wu, P.; Dang, Z. Nickel oxide and carbon nanotube composite (NiO/CNT) as a novel cathode non-precious metal catalyst in microbial fuel cells. *Biosens. Bioelectron.* **2015**, *72*, 332−339.

(82) Modi, A.; Singh, S.; Verma, N. In situ nitrogen-doping of nickel nanoparticle-dispersed carbon nanofiber-based electrodes: Its positive effects on the performance of a microbial fuel cell. *Electrochim. Acta* **2016**, *190*, 620−627.

(83) Ghasemi, M.; Wan Daud, W. R.; Rahimnejad, M.; Rezayi, M.; Fatemi, A.; Jafari, Y.; Somalu, M. R.; Manzour, A. Copper-phthalocyanine and nickel nanoparticles as novel cathode catalysts in microbial fuel cells. *Int. J. Hydrogen Energy* **2013**, *38*, 9533−9540.

(84) Iannaci, A.; Sciarria, T. P.; Mecheri, B.; Adani, F.; Licoccia, S.; D'Epifanio, A. Power generation using a low-cost sulfated zirconium oxide based cathode in single chamber microbial fuel cells. *J. Alloys Compd.* **2017**, *693*, 170−176.

(85) Kodali, M.; Santoro, C.; Serov, A.; Kabir, S.; Artyushkova, K.; Matanovic, I.; Atanassov, P. Air Breathing Cathodes for Microbial Fuel Cell using Mn-, Fe-, Co- and Ni-containing Platinum Group Metal-free Catalysts. *Electrochim. Acta* **2017**, *231*, 115−124.

(86) Rojas-Carbonell, S.; Santoro, C.; Serov, A.; Atanassov, P. Transition metal-nitrogen-carbon catalysts for oxygen reduction reaction in neutral electrolyte. *Electrochem. Commun.* **2017**, *75*, 38−42.

(87) Yang, W.; Logan, B. E. Immobilization of a Metal−Nitrogen−Carbon Catalyst on Activated Carbon with Enhanced Cathode Performance in Microbial Fuel Cells. *ChemSusChem* **2016**, *9*, 2226−2232.

(88) Sebastian, D.; Serov, A.; Artyushkova, K.; Atanassov, P.; Arico, A. S.; Baglio, V. Performance, methanol tolerance and stability of Fe-aminobenzimidazole derived catalyst for direct methanol fuel cells. *J. Power Sources* **2016**, *319*, 235−246.

(89) Sebastián, D.; Serov, A.; Matanovic, I.; Artyushkova, K.; Atanassov, P.; Aricò, A. S.; Baglio, V. Insights on the extraordinary tolerance to alcohols of Fe-N-C cathode catalysts in highly performing direct alcohol fuel cells. *Nano Energy* **2017**, *34*, 195−204.

(90) Rojas-Carbonell, C.; Artyushkova, K.; Serov, A.; Santoro, C.; Matanovic, I.; Atanassov, P. Effect of pH on the Activity of Platinum Group Metal-Free Catalysts in Oxygen Reduction Reaction. *ACS Catal.* **2018**, *8*, 3041−3053.

(91) Santoro, C.; Kodali, M.; Herrera, S.; Serov, A.; Ieropoulos, I.; Atanassov, P. Power generation in microbial fuel cells using platinum group metal-free cathode catalyst: Effect of the catalyst loading on performance and costs. *J. Power Sources* **2018**, *378*, 169−175.

(92) Kodali, M.; Herrera, S.; Kabir, S.; Serov, A.; Santoro, C.; Ieropoulos, I.; Atanassov, P. Enhancement of microbial fuel cell performance by introducing a nano-composite cathode catalyst. *Electrochim. Acta* **2018**, *265*, 56−64.

(93) Leonard, N. D.; Artyushkova, K.; Halevi, B.; Serov, A.; Atanassov, P.; Barton, S. C. Modeling of low-temperature fuel cell electrodes using non-precious metal catalysts. *J. Electrochem. Soc.* **2015**, *162*, F1253−F1261.

(94) Houghton, J.; Santoro, C.; Soavi, F.; Serov, A.; Ieropoulos, I.; Arbizzani, C.; Atanassov, P. Supercapacitive microbial fuel cell:

Characterization and analysis for improved charge storage/delivery performance. *Bioresour. Technol.* **2016**, *218*, 552−560.

(95) Artyushkova, K.; Serov, A.; Rojas-Carbonell, S.; Atanassov, P. Chemistry of Multitudinous Active Sites for Oxygen Reduction Reaction in Transition Metal−Nitrogen−Carbon Electrocatalysts. *J. Phys. Chem. C* **2015**, *119*, 25917−25928.

(96) Hidalgo, D.; Sacco, A.; Hernández, S.; Tommasi, T. Electrochemical and impedance characterization of Microbial Fuel Cells based on 2D and 3D anodic electrodes working with seawater microorganisms under continuous operation. *Bioresour. Technol.* **2015**, *195*, 139−146.

(97) Dominguez-Benetton, X.; Sevda, S.; Vanbroekhoven, K.; Pant, D. The accurate use of impedance analysis for the study of microbial electrochemical systems. *Chem. Soc. Rev.* **2012**, *41*, 7228−7246.

(98) Zhao, F.; Slade, R. C. T.; Varcoe, J. R. Techniques for the study and development of microbial fuel cells: an electrochemical perspective. *Chem. Soc. Rev.* **2009**, *38*, 1926−1939.

(99) Santini, M.; Marzorati, S.; Fest-Santini, S.; Trasatti, S.; Cristiani, P. Carbonate scale deactivating the biocathode in a microbial fuel cell. *J. Power Sources* **2017**, *356*, 400−407.

(100) Santini, M.; Guilizzoni, M.; Lorenzi, M.; Atanassov, P.; Marsili, E.; Fest-Santini, S.; Cristiani, P.; Santoro, C. Three-dimensional X-ray microcomputed tomography of carbonates and biofilm on operated cathode in single chamber microbial fuel cell. *Biointerphases* **2015**, *10*, 031009.

(101) Oliot, M.; Galier, S.; Roux de Balmann, H.; Bergel, A. Ion transport in microbial fuel cells: Key roles, theory and critical review. *Appl. Energy* **2016**, *183*, 1682−1704.

(102) Zhou, L.; Liao, C.; Li, T.; An, J.; Du, Q.; Wan, L.; Li, N.; Pan, X.; Wang, X. Regeneration of activated carbon air-cathodes by half-wave rectified alternating fields in microbial fuel cells. *Appl. Energy* **2018**, *219*, 199−206.

(103) Zhang, X.; Pant, D.; Zhang, F.; Liu, J.; He, W.; Logan, B. E. Long-Term Performance of Chemically and Physically Modified Activated Carbons in Air Cathodes of Microbial Fuel Cells. *ChemElectroChem* **2014**, *1*, 1859−1866.

(104) Larrosa-Guerrero, A.; Scott, K.; Head, I. M.; Mateo, F.; Ginesta, A.; Godinez, C. Effect of temperature on the performance of microbial fuel cells. *Fuel* **2010**, *89*, 3985−3994.

(105) Behera, M.; Murthy, S. S.; Ghangrekar, M. M. Effect of operating temperature on performance of microbial fuel cell. *Water Sci. Technol.* **2011**, *64*, 917−922.

(106) Rossi, R.; Yang, W.; Setti, L.; Logan, B. E. Assessment of a metal−organic framework catalyst in air cathode microbial fuel cells over time with different buffers and solutions. *Bioresour. Technol.* **2017**, *233*, 399−405.

(107) Martin, E.; Tartakovsky, B.; Savadogo, O. Cathode materials evaluation in microbial fuel cells: A comparison of carbon, Mn_2O_3, Fe_2O_3 and platinum materials. *Electrochim. Acta* **2011**, *58*, 58−66.

(108) Rossi, R.; Yang, W.; Zikmund, E.; Pant, D.; Logan, B. E. In-situ biofilm removal from air cathodes in microbial fuel cells treating domestic wastewater. *Bioresour. Technol.* **2018**, *265*, 200−206.